

Single crystal growth by self-flux method of the mixed valence gold halides $\text{Cs}_2[\text{Au}^I\text{X}_2][\text{Au}^{III}\text{X}_4]$ (X=Br,I)

Scott C. Riggs, M. C. Shapiro, F. Corredor, T. H. Geballe, I. R. Fisher
Department of Applied Physics and Geballe Laboratory for Advanced Materials, Stanford University, CA 94305.

Gregory T. McCandless, Julia Y. Chan
Department of Chemistry, Louisiana State University, Baton Rouge, LA 70803
(Dated: November 27, 2024)

High quality single crystals of $\text{Cs}_2\text{Au}_2\text{X}_6$ (X=Br,I) were grown using a ternary self-flux method. Structural refinements based on single crystal X-ray diffraction measurements show that both materials have a distorted perovskite structure belonging to the $I4/mmm$ space group with full site occupancy. Transport measurements reveal a large bandgap of 550 ± 100 meV for $\text{Cs}_2\text{Au}_2\text{I}_6$ and 520 ± 80 meV for $\text{Cs}_2\text{Au}_2\text{Br}_6$. Initial attempts at chemical substitution are described.

PACS numbers: ???, ???, ???

I. INTRODUCTION

The title compounds, $\text{Cs}_2\text{Au}_2\text{X}_6$ (X=Br,I) adopt a distorted perovskite structure. Although simple charge counting arguments might indicate a single gold valence Au^{II} , and hence a metallic state, the materials are in fact found to be hard insulators, comprising two distinct Au sites with different formal valences Au^I and Au^{III-5} . However, hydrostatic pressure can induce a coupled first order structural and valence transition at ≈ 9 GPa for X=Br and ≈ 5.5 GPa for X=I, spurring considerable recent interest in the associated changes in the electronic behavior^{3,6,7}.

The mixed valence state in $\text{Cs}_2\text{Au}_2\text{X}_6$ at ambient pressure is reminiscent of $\text{Ba}_2\text{Bi}_2\text{O}_6$, which also adopts a distorted perovskite structure in which two distinct Bi sites have been associated with formal valences Bi^{III} and Bi^{V8} . Significantly, in the case of $\text{Ba}_2\text{Bi}_2\text{O}_6$, suppression of the charge density wave (CDW) state via hole doping yields superconducting ground states for $\text{Ba}_{2-x}\text{K}_x\text{Bi}_2\text{O}_6$ ^{9,10} and $\text{Ba}_2\text{Bi}_{2-x}\text{Pb}_x\text{O}_6$ ¹¹ with moderately high maximum T_c values of 30 and 12 K, respectively. The origin of the pairing interaction in these compounds is unclear and is still a matter of ongoing research. One possibility that has been suggested is that the correlations that result in CDW formation for the parent compound are still present for the doped materials, and that the associated valence fluctuations in the metallic regime result in a local pairing interaction¹². Some evidence such a scenario might be appropriate can be found in the doped superconducting semiconductor $\text{Pb}_{1-x}\text{Tl}_x\text{Te}$, for which Kondo-like behavior in the absence of magnetic impurities has been attributed to Tl valence fluctuations¹³⁻¹⁵. The physical origin of the charge disproportionation in these materials is likely somewhat different, though. In the case of $\text{Ba}_2\text{Bi}_2\text{O}_6$ and Tl-doped PbTe, the two valence states are associated with filled and empty 6s shells, whereas for $\text{Cs}_2\text{Au}_2\text{X}_6$ Jahn-Teller distortion of the coordinating halogen ligands stabilizes $5d^8$ and $5d^{10}$ electron configurations. Nevertheless, the

fact that charge disproportionation plays an important role for both materials motivates a concerted experimental effort aimed at suppressing the mixed valence CDW state in $\text{Cs}_2\text{Au}_2\text{X}_6$ via chemical substitution. Controllable chemical substitution requires a synthesis technique that readily allows additional elements to be introduced in a controlled fashion.

Previously, single crystals of $\text{Cs}_2\text{Au}_2\text{X}_6$ (X = Br and I) have been grown via a diffusion method, using either acetonitrile or hydriodic acid as a solvent respectively^{7,16}. This technique suffers the drawback of not being easy to introduce additional elements to the solution, motivating development of alternative crystal growth techniques. Here we show how large, high quality single crystals of $\text{Cs}_2\text{Au}_2\text{X}_6$ can be grown directly from a ternary melt via a slow-cooling, self flux technique. We characterize the samples by single crystal x-ray diffraction, electron microprobe analysis, and electrical transport measurements. We also describe results of initial attempts at chemical substitution.

II. SYNTHESIS

The largest crystals of $\text{Cs}_2\text{Au}_2\text{I}_6$ were obtained by slow cooling mixtures of CsI (Alfa, 99.999%), Au (Alfa, .99%), and I_2 (Alfa, 99.99%) in molar ratios of 1.3:1:1 respectively. The reagents were weighed and placed in a 2 ml alumina crucible, which was then sealed in a quartz tube after being flushed with argon and evacuated. The quantity of reagents was calculated such that the pressure in the quartz tube would not exceed 3 atm at the maximum temperature. For $\text{Cs}_2\text{Au}_2\text{Br}_6$, optimal results were obtained from a similar molar ratio of reagents (CsBr: Alfa, 99.999%), but liquid bromine (Alfa, 99.998%) was added to the crucible inside the quartz tube using a micro-pipette *after* the tube was partially necked using a hydrogen torch to minimize loss of bromine. The end of the quartz tube holding the crucible was then cooled by immersion in liquid nitrogen to avoid evaporation of

Br during the evacuation and subsequent sealing of the ampoule. The sealed quartz tubes were placed in a furnace and heated from room temperature to 630°C for $\text{Cs}_2\text{Au}_2\text{Br}_6$ and 550°C for $\text{Cs}_2\text{Au}_2\text{I}_6$ over the course of 42 hours. After dwelling for 10 hours, the furnace was allowed to cool back to room temperature at a rate of 5 C/hr. Crystal growth does not appear to occur via chemical vapor transport, but rather via precipitation from the molten solution. Care must be taken when opening the quartz tube after the growth procedure since small quantities of unreacted Cs can sometimes react violently when exposed to oxygen. Crystals with dimensions up to approximately $600\mu\text{m} \times 300\mu\text{m} \times 50\mu\text{m}$ can be readily extracted from the crucible. The crystals have a platelike morphology, with the c-axis perpendicular to the plane of the plate and are gold in color (Figure 1). The material reacts with moisture, and must be stored in a desiccator.

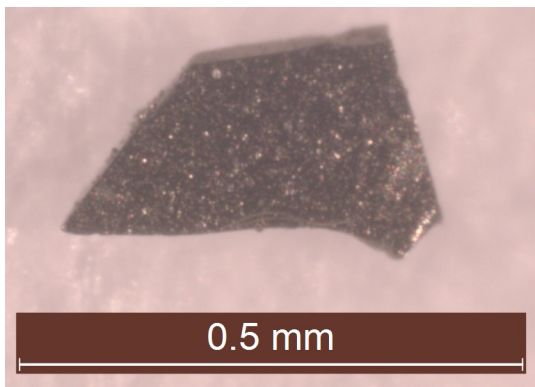


FIG. 1. Photograph of a representative single crystal of $\text{Cs}_2\text{Au}_2\text{I}_6$ grown via a self flux. The crystals form as thin plates, with the c-axis perpendicular to the plane of the plates, and are gold in color.

The crystal growth method described above readily enables incorporation of a wide variety of additional elements to the melt. Initial substitution experiments included Zn, Ga, Se, Ag, Cd, In, Te, Pt, Pb, Bi and Ho, for a variety of concentrations. In all cases, the additional elements appeared to dissolve in the melt. And in nearly all cases, slow cooling of the quaternary melt still resulted in crystal growth of $\text{Cs}_2\text{Au}_2\text{X}_6$, though often with slightly reduced size. However, microprobe analysis revealed that none of these elements were incorporated into the $\text{Cs}_2\text{Au}_2\text{X}_6$ crystal lattice to any appreciable extent. Furthermore, electrical resistivity measurements for crystals taken from these batches always revealed insulating behavior with a similar gap to that of the parent compounds (see section IV below). Hence, despite considerable effort, we have thus far been unable to make $\text{Cs}_2\text{Au}_2\text{X}_6$ metallic by chemical substitution. The list of elements that we have been able to try thus far is certainly not exhaustive, and several other impurities and other strategies (including high pressure synthesis) might be more favorable.

The remainder of the paper is dedicated to the characterization of the undoped parent compounds grown from ternary melts as described above.

III. CRYSTAL STRUCTURE

Initial powder x-ray diffraction measurements indicated a similar structure to previous measurements of $\text{Cs}_2\text{Au}_2\text{X}_6$ ³. For a full structure determination, crystallographic data was collected using a Nonius KappaCCD X-ray diffractometer equipped with a Mo $K\alpha$ radiation source ($\lambda = 0.71073$ angstrom) and a graphite monochromator. For $\text{Cs}_2\text{Au}_2\text{I}_6$, a crystal with dimensions $\approx 0.05\text{mm} \times 0.35\text{mm} \times 0.45\text{mm}$ was mounted on a thin glass fiber using epoxy as an adhesive and diffraction data was collected out to 2θ of 80 degrees. The data collection strategy (a combination of ϕ and ω scans) was developed based on preliminary frames collected for unit cell determination and the criteria of a desired dataset completeness of 99.995% and redundancy of 3. Unit cell parameters and systematic absences suggested that the structure is body-centered tetragonal. Absorption was corrected using the multi-scan correction¹⁷. After determining the space group with the maXus software package, a preliminary model was generated using SIR97¹⁸. Final least-squares refinement of the model and extinction correction was carried out in SHELXL-97 and missing symmetry was evaluated with PLATON^{19,20}. The best fitting space group for $\text{Cs}_2\text{Au}^I\text{Au}^{III}\text{I}_6$ is $I4/mmm$ (No. 139) and our model agrees with previous structure report for this compound³.

A similar structure determination was also performed for $\text{Cs}_2\text{Au}^I\text{Au}^{III}\text{Br}_6$ using x-ray diffraction data collected with a smaller single crystal, $\approx 0.02\text{mm} \times 0.1\text{mm} \times 0.2\text{mm}$). The best fitting space group for $\text{Cs}_2\text{Au}^I\text{Au}^{III}\text{Br}_6$ is also $I4/mmm$ (No. 139) and coincides with previous structure reports for this compound²¹.

Details of the structural refinement for both compounds are listed in Tables I-IV. For both cases, the x-ray refinement indicates full site occupancy. For $\text{Cs}_2\text{Au}_2\text{I}_6$, the cation stoichiometry was also checked by electron microprobe analysis, using a JEOL JXA-733A with elemental Cs and Au standards. Normalized to the Cs content, the Au content was found to be 1.004 ± 0.032 , confirming the full site occupancy determined by x-ray diffraction. Uncertainties represent the standard deviation between multiple measurements on the same crystal performed at different crystallographic locations. The iodine concentration could not be accurately determined due to partial decomposition in the electron beam, presumably due to heating effects.

As illustrated in Fig.2, the $\text{Cs}_2\text{Au}_2\text{X}_6$ structure comprises a distorted perovskite structure in which linearly coordinated AuX_2 and square-planar coordinated AuX_4 complexes alternate through the crystal lattice. Interatomic distances are listed in Table IV. As previously

suggested, the coordination is typical of Au^I and Au^{III} formal valences respectively^{7,21}. The ratios of short-to-long Au-X bonds $\frac{\text{Au1-X1}}{\text{Au1-X2}}$ and $\frac{\text{Au2-X2}}{\text{Au2-X1}}$ is slightly closer to unity for X = I (0.7631 and 0.8017 respectively) than for Br (0.7464 and 0.7883). This difference can also be appreciated by inspection of the internal parameters describing the positions of the halogen ions X1 and X2 in the unit cell (Table III), which are closer to the fully symmetric positions (0.25, 0.25, 0) and (0.5, 0.5, 0.25) respectively for X = I than for X = Br. This difference is likely directly related to the reduced value of the critical pressure associated with the coupled valence and structural transition found for $\text{Cs}_2\text{Au}_2\text{I}_6$ (≈ 5.5 GPa) relative to $\text{Cs}_2\text{Au}_2\text{Br}_6$ (≈ 9 GPa), but the physical origin of the difference is unclear.

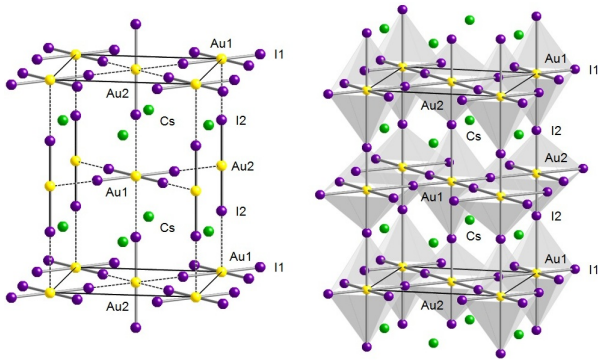


FIG. 2. Crystal structure of the distorted perovskite $\text{Cs}_2\text{Au}^I\text{Au}^{III}\text{I}_6$. Cs and Au sites are labeled; X sites are shown by purple spheres. The left hand panel shows the square planar Au^{II}I_4 and linear chain Au^II_2 complexes associated with the Au1 and Au2 sites respectively. The right hand panel emphasizes the distorted octahedral coordination of the two sites (compressed octahedral coordination for the $(\text{Au}^I\text{I}_2)^-$ chains versus elongated octahedral coordination for the $(\text{Au}^{III}\text{I}_4)^-$ square planar complexes). The tetragonal c-axis is vertical.

IV. ELECTRICAL RESISTIVITY

Transport measurements were made on single crystals of $\text{Cs}_2\text{Au}_2\text{X}_6$ using a Keithley electrometer. Samples were mounted in a 2-wire configuration for measurement of the in-plane resistivity. Contacts were made with Au wires using Dupont 4929 Ag-epoxy and allowed to set at room temperature. Samples were attached to a glass slide and wired to an Oxford Instruments optiflow cryostat probe with two separated coaxial cables. The inner cores of the coaxial cables were used for the voltage measurement. Measurements were made over a temperature range of roughly 300K to 200K with the sample in He exchange gas. Below $\approx 200\text{K}$ the resistivity became too large and was no longer measurable using the current experimental set-up.

TABLE I. Crystallographic Parameters

<i>Crystal data</i>		
Formula	$\text{Cs}_2\text{Au}_2\text{I}_6$	$\text{Cs}_2\text{Au}_2\text{Br}_6$
$M_r(\text{g mol}^{-1})$	1421.15	1139.21
Crystal system	Tetragonal	Tetragonal
Space group	I4/mmm	I4/mmm
$a(\text{\AA})$	8.2847(10)	7.7869(10)
$c(\text{\AA})$	12.0845(15)	11.3808(15)
$V(\text{\AA}^3)$	829.43(18)	690.08(15)
Z	2	2
F(000)	1172	956
$D_X(\text{g cm}^{-3})$	5.690	5.483
2θ range($^\circ$)	5.2-55.0	2.0-80.6
$\mu(\text{mm}^{-1})$	33.12	43.75
Temperature (K)	298(2)	298(2)
Mosaicity ($^\circ$)	0.494(1)	0.544(2)
<i>Data collection</i>		
Measured reflections	948	2183
Independent reflections	306	669
Reflections with $I > 2\sigma(I)$	301	505
$^a R_{int}$	0.026	0.036
h	-10 \rightarrow 10	-14 \rightarrow 14
k	-7 \rightarrow 7	-9 \rightarrow 10
l	-15 \rightarrow 15	-20 \rightarrow 20
<i>Refinement</i>		
Reflections	306	669
Parameters	15	15
$^b R_1[F^2 > 2\sigma(F^2)]$	0.048	0.028
$^c wR_2(F^2)$	0.130	0.075
$^d S$	1.23	1.06
$\Delta\rho_{max}(\text{e}\text{\AA}^{-3})$	2.90	1.53
$\Delta\rho_{min}(\text{e}\text{\AA}^{-3})$	-5.39	-2.97
Extinction coefficient	0.0034(5)	0.00157(15)

$$^a R_{int} = [\sum |F_o^2 - F_c^2(\text{mean})| / \sum F_o^2]$$

$$^b R_1 = \frac{||F_o| - |F_c||}{\sum |F_o|}$$

$$^c wR_2 = \left\{ \frac{\sum [w(F_o^2 - F_c^2)^2]}{\sum [w(F_o^2)^2]} \right\}^{\frac{1}{2}},$$

$$w = 1 / [\sigma^2(F_o^2) + (0.0995P)^2 + 0.8069P] \text{ for } \text{Cs}_2\text{Au}_2\text{I}_6$$

$$w = 1 / [\sigma^2(F_o^2) + (0.0356P)^2 + 2.4804P] \text{ for } \text{Cs}_2\text{Au}_2\text{Br}_6$$

$$^d S = \left\{ \frac{\sum [w(F_o^2 - F_c^2)^2]}{(n-p)} \right\}^{\frac{1}{2}}$$

The temperature dependence of the resistivity of both compounds follows an activated behavior, which can be readily appreciated by inspection of figure 3 showing the natural log of the resistance as a function of inverse temperature. Data plotted in this manner were fit to a straight line and the gap Δ determined assuming typical semiconductor activated behavior:

$$R = R_0 e^{\frac{\Delta}{2k_B T}} \quad (1)$$

Resulting values of the bandgap are, $\Delta_I = 550 \pm 100$ meV and $\Delta_{Br} = 520 \pm 80$ meV for $\text{Cs}_2\text{Au}_2\text{I}_6$ and $\text{Cs}_2\text{Au}_2\text{Br}_6$, respectively, where the relatively large uncertainty reflects a combination of electrical contact to the material and sample-to-sample variation.

The gold-halide materials are very good insulators, with a typical room temperature resistivity of ≈ 700 m Ω

TABLE II. Selected Interatomic Distances (\AA)

Cs-I1 (x8)	4.2175(4)
Cs-I2 (x4)	4.1662(5)
Au1-I1 (x4)	2.6454(13)
Au1-I2 (x2)	3.4666(14)
Au2-I1 (x4)	3.2128(13)
Au2-I2 (x2)	2.5757(14)
<hr/>	
Au1 \rightarrow Au2 (along ab plane)	5.8582(7)
Au1 \rightarrow Au2 (along c axis)	6.0423(8)
<hr/>	
Cs-Br1(x8)	3.9709(4)
Cs-Br2(x4)	3.9175(5)
Au1-Br1(x4)	2.4471(9)
Au1-Br2(x2)	3.2787(13)
Au2-Br1(x4)	3.0591(10)
Au2-Br2(x2)	2.4117(13)
Au1 \rightarrow Au2 (along ab plane)	5.5062(5)
Au1 \rightarrow Au2 (along c axis)	5.6904(8)

cm, corresponding to resistances of 500 M Ω for typical sample dimensions. The measured transport gap (550 meV for X=I) is considerably less than estimates of the minimum intervalence charge transfer (IVCT) excitation determined from optical reflectivity measurements (\approx 806 meV for the Au^I(5d_{z²) to Au^{III}(5d_{x²-y²) transition for Cs₂Au₂I₆ observed for electric fields oriented perpendicular to the crystallographic c-axis) determined from optical reflectivity measurements⁶.}}

The reason for this difference is not immediately obvious. Given the very large value of the intrinsic resistance of the samples (rising up to 25 G Ω at \approx 200K for typical samples), the discrepancy might be due to excess halogen leaching out of the crystals, or water settling on the sample surface, affecting current paths and

lowering the effective gap. Unfortunately, the surfaces could not be easily cleaned with usual solvents, including water, methanol, acetone, and isopropyl alcohol, due to adverse reaction. Equally, a difference in the apparent gap probed by transport and reflectivity measurements can arise from a number of mechanisms including an indirect bandgap, pinning of the chemical potential by localized impurity states, or perhaps if the charge transport mechanism does not involve single carrier hopping. Perhaps coincidentally, the closely related CDW compound Ba₂Bi₂O₆ also exhibits a significant difference in the transport and optical gap (by a factor of almost ten)²², although the origin of this effect is uncertain.

V. CONCLUSIONS

In conclusion, we have described an alternative method to grow large, high quality, single crystals of the mixed valence compounds Cs₂Au^IAu^{III}X₆, (X=I,Br) by means of a ternary self-flux. Single crystals x-ray diffraction measurements confirmed the previously determined crystal structure of both compounds^{3,21}. Transport measurements reveal a band gap of 550 \pm 100 meV for Cs₂Au₂I₆ and 520 \pm 80 meV for Cs₂Au₂Br₆. Initial attempts to chemically substitute with a variety of dopants, were unsuccessful.

VI. ACKNOWLEDGMENTS

Scott Riggs would like to thank R. Jones for microprobe analysis. Work at Stanford University was supported by the AFOSR grant FA9550-09-1-0583. Work at LSU was supported by NSF grant DMR 1063735.

-
- ¹ H. Tanino and K. Takahashi, Solid State Communications **59**, 825 (1986).
² H. Kitagawa, N. Kojima, and T. Nakajima, J. Chem. Soc. , 3121 (1991).
³ N. Matsushita, H. Kitagawa, and N. Kojima, Acta Crystallogr. Sect. C **53**, 663 (1997).
⁴ K. Ikeda, K. Kojima, Y. Ono, Y. Kobayashi, M. Seto, X. J. Liu, and Y. Moritomo, Hyperfine Interactions **156**, 311 (2004).
⁵ L. Xiao-Jun, M. Yutaka, and N. Kojima, Chin. Phys. Lett. **21**, 183 (2004).
⁶ X. J. Liu, K. Matsuda, Y. Moritomo, A. Nakamura, and N. Kojima, Phys. Rev. B **59**, 7925 (1999).
⁷ N. Kojima, Bull. Soc. Jpn. **73**, 1445 (2000).
⁸ D. E. Cox and A. Sleight, Acta Cryst **B35**, 1 (1979).
⁹ R. J. C. et al, Nature **332**, 814 (1988).
¹⁰ S. Pei, J. D. Jorgensen, B. Dabrowski, D. G. Hinks, D. R. Richards, A. W. Mitchell, J. M. Newsam, S. K. Sinha, D. Vaknin, and A. J. Jacobson, Phys. Rev. B **41**, 4126 (1990).
¹¹ A. W. S. et al, Solid State Commun. **17**, 27 (1975).
¹² C. Varma, Phys. Rev. Lett. **61**, 2173 (1988).
¹³ Y. Matsushita, H. Bluhm, T. H. Geballe, and I. R. Fisher, Phys. Rev. Lett. **94**, 157002 (2005).
¹⁴ M. Matusiak, E. M. Tunncliffe, J. R. Cooper, Y. Matsushita, and I. R. Fisher, Phys. Rev. B **80**, 220403 (2009).
¹⁵ M. Dzero and J. Schmalian, Phys. Rev. Lett. **94**, 157003 (2005).
¹⁶ A. Rabenau and H. Rau, Inorg. Syntheses XIV **160** (2003).
¹⁷ Z. Otwinowski and W. Minor (Academic Press Inco, 1997) pp. 307–326.
¹⁸ A. Altomare, M. C. Burla, M. Camalli, G. L. Cascarano, C. Giacovazzo, A. Guagliardi, A. G. G. Moliterni, G. Polidori, and R. Spagna, J. Appl. Crystallogr. , 115 (1999).
¹⁹ G. M. Sheldrick, Acta Crystallogr. , 112 (2008).
²⁰ A. L. Spek, J. Appl. Crystallogr. **36**, 7 (2003).
²¹ N. Matsushita, F. Fukuhara, and N. Kojima, Acta Crystallogr. **61**, i123 (2005).
²² S. Tajima, S. Uchida, A. Masaki, H. Takagi, K. Kitazawa, S. Tanaka, and S. Sugai, Phys. Rev. B **35**, 696 (1987).

TABLE III. Atomic Positions and Equivalent Isotropic Displacement Parameters

Atom	Wyckoff position	x	y	z	^a Occ.	^b U _{eq} (Å ²)
Cs	4d	0	$\frac{1}{2}$	$\frac{1}{4}$	1	0.0543(8)
Au1(+3)	2a	0	0	0	1	0.0226(5)
Au2(+1)	2b	$\frac{1}{2}$	$\frac{1}{2}$	0	1	0.0269(5)
I1	8h	0.22578(11)	0.22578(11)	0	1	0.0423(6)
I2	4e	$\frac{1}{2}$	$\frac{1}{2}$	0.21314(11)	1	0.0381(6)
Cs	4d	0	$\frac{1}{2}$	$\frac{1}{4}$	1	0.0466(2)
Au1(+3)	2a	0	0	0	1	0.02299(13)
Au2(+1)	2b	$\frac{1}{2}$	$\frac{1}{2}$	0	1	0.02541(14)
Br1	8h	0.22221(8)	0.22221(8)	0	1	0.0402(2)
Br2	4e	1/2	1/2	0.21191(11)	1	0.0385(3)

^aOccupancy of atoms^bU_{eq} is defined as one-third of the trace of the orthogonalized U^{ij} tensorTABLE IV. Anisotropic Atomic Displacement Parameters (Å²)

Atom	U ¹¹	U ²²	U ³³	U ¹²	U ¹³	U ²³
Cs	0.0537(11)	0.0537(11)	0.0553(15)	0.000	0.000	0.000
Au1	0.0232(6)	0.0232(6)	0.0215(8)	0.000	0.000	0.000
Au2	0.0318(6)	0.0318(6)	0.0169(7)	0.000	0.000	0.000
I1	0.0376(7)	0.0376(7)	0.0518(9)	-0.0140(5)	0.000	0.000
I2	0.0485(8)	0.0485(8)	0.0173(9)	0.000	0.000	0.000
Cs	0.0461(3)	0.0461(3)	0.0475(5)	0.000	0.000	0.000
Au1	0.02288(16)	0.02288(16)	0.0232(2)	0.000	0.000	0.000
Au2	0.02714(17)	0.02714(17)	0.0219(2)	0.000	0.000	0.000
Br1	0.0358(3)	0.0358(3)	0.0490(5)	-0.0118(3)	0.000	0.000
Br2	0.0468(4)	0.0468(4)	0.0220(4)	0.000	0.000	0.000

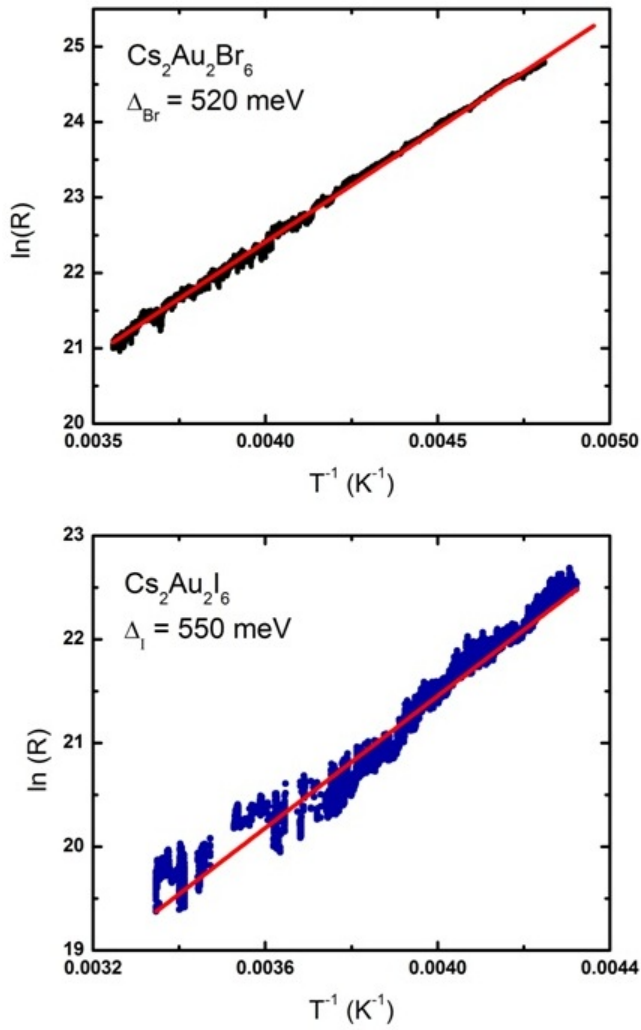


FIG. 3. Arhenius plots showing activated behavior of the in-plane resistance of representative single crystals of (a) $\text{Cs}_2\text{Au}_2\text{Br}_6$ and (b) $\text{Cs}_2\text{Au}_2\text{I}_6$. Red lines show linear fits, yielding gaps of Δ_{I} is $550 \pm 100 \text{ meV}$ and Δ_{Br} is $520 \pm 80 \text{ meV}$.